

Multiple magnetic phases and magnetization plateaus in TbRh_6Ge_4

Yuxin Chen,¹ Yongjun Zhang,² Rui Li,¹ Hang Su,¹ Zhaoyang Shan,¹ Michael Smidman^{1,*} and Huiqiu Yuan^{1,3,4,†}

¹Center for Correlated Matter and School of Physics, Zhejiang University, Hangzhou 310058, China

²Institute for Advanced Materials, Hubei Normal University, Huangshi 435002, China

³State Key Laboratory of Silicon Materials, Zhejiang University, Hangzhou 310058, China

⁴Collaborative Innovation Center of Advanced Microstructures, Nanjing University, Nanjing 210093, China



(Received 21 December 2022; revised 21 February 2023; accepted 28 February 2023; published 14 March 2023)

We probe the magnetic order in single crystals of TbRh_6Ge_4 using electrical transport, magnetization, and thermodynamic measurements. TbRh_6Ge_4 crystallizes in the noncentrosymmetric tetragonal LiCo_6P_4 -type structure, where the Tb ions form a triangular lattice in the basal plane and chains along the c axis. This compound undergoes a second-order antiferromagnetic transition at $T_N = 12.7$ K, which is followed by an additional transition at $T_M = 2.8$ K. When fields are applied along the easy c axis, multiple metamagnetic transitions are observed, where there are plateaus at $1/9$ and $1/3$ of the saturation magnetization. We map the field-temperature phase diagram revealing complex magnetism, where antiferromagnetic coupling within the basal plane may lead to significant magnetic frustration.

DOI: [10.1103/PhysRevB.107.094414](https://doi.org/10.1103/PhysRevB.107.094414)

I. INTRODUCTION

In frustrated magnetic systems, the inability to satisfy all the competing magnetic exchange interactions can prevent the formation of long-range magnetic order, leading to unusual correlated phases such as spin liquids with fractionalized excitations [1,2]. In other instances there is still magnetic ordering, yet frustration can still have a profound impact on the magnetic properties [3], giving rise to a range of phenomena including magnetization plateaus in applied fields [4–8], the anomalous Hall effect [9–11], and the spin-Jahn-Teller effect [12–14]. Magnetization plateaus generally occur at rational fractions of the saturation magnetization, and can occur in a variety of frustrated geometries, including triangular [15–17], Shastry-Sutherland-type [18,19], square [20,21], and kagome lattices [22–26]. Such plateaus arise in a variety of contexts, including in systems with very weak magnetic anisotropy induced by spin-phonon coupling [27,28], and in low-dimensional spin systems such as those with interacting spin chains [29–34]. Rare-earth-based intermetallic compounds with triangular or kagome lattices, where $4f$ ions interact via long-range magnetic exchange interactions, can also host an analogous range of frustration-induced behaviors, where magnetization plateaus can arise in the context of uniaxial [35,36] or planar [37] magnetocrystalline anisotropies, as well as multi-Q and mixed magnetic structures [38].

The intermetallic materials $RE\text{Rh}_6\text{Ge}_4$ ($RE = \text{Ce-Sm, Gd-Yb}$) crystallize in the noncentrosymmetric LiCo_6P_4 -type structure (space group $P6m2$) displayed in Fig. 1(a) [39,40]. Here the rare-earth atoms form a triangular lattice in the basal

plane, and their spacing along the c axis is much smaller than in the plane, suggesting a possible quasi-one-dimensional (q1D) structure with rare-earth chains. CeRh_6Ge_4 , a Kondo ferromagnet with $T_C = 2.5$ K [41], is a rare example of a clean stoichiometric ferromagnet exhibiting a pressure-induced ferromagnetic (FM) quantum critical point [42,43], which is accompanied by a strange metal phase with a T -linear resistivity and a logarithmic divergence of the specific heat coefficient [42]. Angle-resolved photoemission spectroscopy (ARPES) reveals q1D hybridization between the $4f$ and the conduction electrons, which is much stronger along the Ce chains than in the basal plane [44], and may be facilitated by the anisotropy of the crystalline-electric field (CEF) ground state orbitals [45].

Given the q1D chain-like structure and anisotropic couplings in CeRh_6Ge_4 , it is of particular interest to explore the magnetism of other $RE\text{Rh}_6\text{Ge}_4$ systems. This especially applies to antiferromagnetic compounds in this series, since antiferromagnetic interactions on a triangular lattice can give rise to geometric frustration. Previously, antiferromagnetic transitions have been found in GdRh_6Ge_4 (8.4 K), TbRh_6Ge_4 (13.6 K), DyRh_6Ge_4 (5.1 K), and YbRh_6Ge_4 (8.9 K) [40], but only limited measurements on polycrystalline samples are reported.

In this paper we report the synthesis of single crystals of TbRh_6Ge_4 using a Bi flux, and we investigate the magnetic properties by measuring the electrical resistivity, specific heat, and magnetization. As well as the previously reported antiferromagnetic transition at $T_N = 12.7$ K, we also observe a second transition in zero field below $T_M = 2.8$ K, which also has a ferromagnetic component. Field-dependent measurements reveal various metamagnetic transitions with plateaus in the magnetization, pointing to a complex H - T phase diagram likely related to antiferromagnetic coupling between Tb chains.

*msmidman@zju.edu.cn

†hqyuan@zju.edu.cn

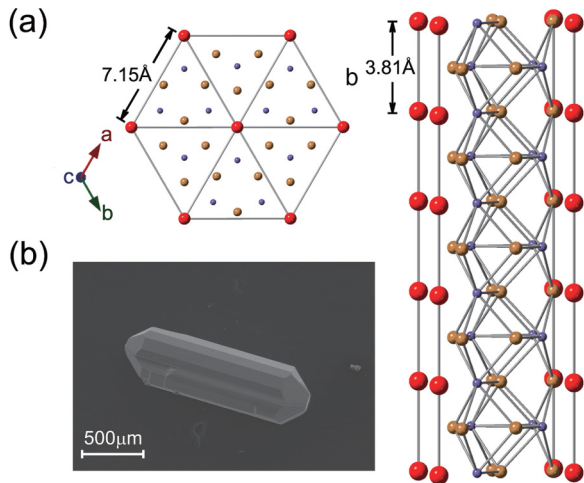


FIG. 1. (a) Crystal structure of TbRh_6Ge_4 , where red, purple, and brown atoms represent Tb, Rh, and Ge atoms, respectively. (b) Scanning electron microscope image showing the morphology of a typical TbRh_6Ge_4 crystal.

II. EXPERIMENTAL METHODS

Single crystals of TbRh_6Ge_4 were grown using a Bi flux. The starting materials, Tb (pieces, Alfa 99.9%), Rh (powder, PrMat 99.95%), Ge (ingots, Alfa 99.9999%), and Bi (granules, Alfa 99.997%), were placed in an alumina crucible in a molar ratio of Tb:Rh:Ge:Bi = 1:6:4:100 and sealed in an evacuated quartz ampoule. The ampoule was heated to 1373 K, held at this temperature for 10 h, and was then cooled to 773 K at a rate of 2 K h^{-1} , after which the bismuth was separated from the crystals by centrifuging. Residual bismuth was dissolved in a 1:1 molar mixture of H_2O_2 and acetic acid. Needle-like crystals with typical lengths of 0.3–1.3 mm were obtained, as shown in Fig. 1(b). The chemical composition was checked using energy-dispersive x-ray analysis with a Hitachi SU-8010 field emission scanning electron microscope, revealing an atomic ratio of Tb:Rh:Ge of 0.97:5.97:4, which is close to 1:6:4. The crystal structure was characterized using single-crystal x-ray diffraction (XRD) with an XtaLAB Synergy-I diffractometer with $\text{Cu K}\alpha_1$ radiation, yielding lattice parameters of $a = 7.1524(14)$ Å and $c = 3.8126(14)$ Å, consistent with previous reports [40]. The magnetization and magnetic susceptibility measurements were performed using a Quantum Design Magnetic Property Measurement System (QD MPMS-5T). The specific heat was measured down to 0.4 K using the relaxation method in a Quantum Design Physical Property Measurement System (PPMS), while the electrical resistivity was measured using a four-probe technique in the PPMS.

III. RESULTS AND DISCUSSION

A. Magnetic transitions in TbRh_6Ge_4

The temperature dependence of the electric resistivity $\rho(T)$ measured with the current parallel to the c axis is displayed in Fig. 2(a). At low temperatures, $\rho(T)$ shows a peak at the antiferromagnetic ordering temperature $T_N \approx 12.7$ K, consistent with previous reports [40], and there is another peak at lower

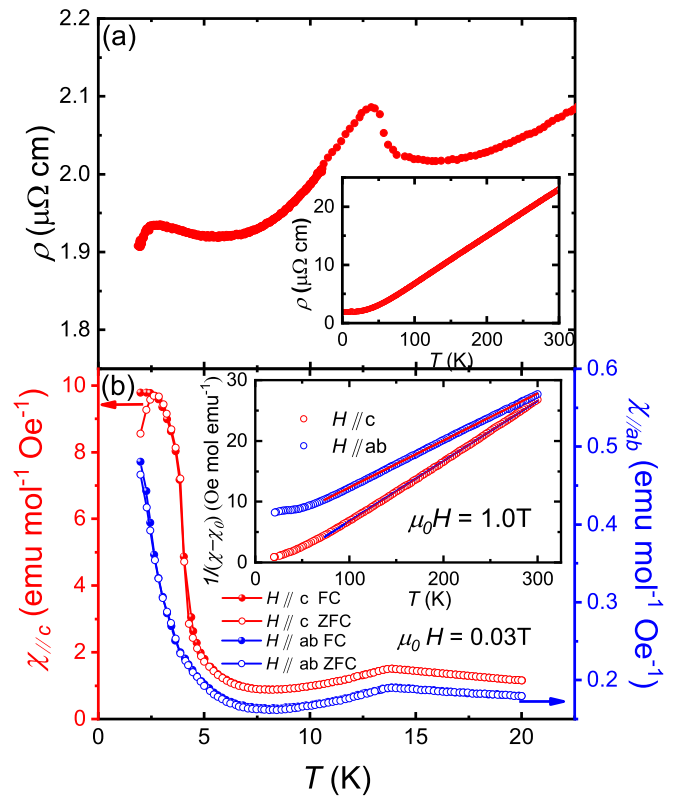


FIG. 2. (a) Temperature dependence of the resistivity $\rho(T)$ of TbRh_6Ge_4 in the temperature range 2–25 K. The insets display $\rho(T)$ for 2–300 K. (b) Temperature dependence of the magnetic susceptibility $\chi(T)$ of TbRh_6Ge_4 in the temperature range 2–20 K, measured upon both ZFC and FC in applied fields of 0.03 T both parallel to the c axis (left axis) and in the ab plane (right). The inset shows $1/(\chi - \chi_0)$, where the solid lines correspond to fitting with the Curie-Weiss law.

temperatures at $T_M \approx 2.8$ K. The inset of Fig. 2(a) shows $\rho(T)$ in the range of 2–300 K. The nearly linear $\rho(T)$ above 100 K likely arises from electron-phonon scattering [46].

Figure 2(b) displays the temperature dependence of the magnetic susceptibility $\chi(T)$ of TbRh_6Ge_4 , measured in an applied field of $\mu_0 H = 0.03$ T both parallel to the c axis and within the ab plane. The low temperature $\chi(T)$ for $H \parallel c$ and $H \parallel ab$ both exhibit a peak at T_N . At lower temperatures there is a considerable increase of $\chi(T)$ along both directions, and for $H \parallel c$ in the field-cooled (FC) case, $\chi(T)$ begins to saturate at the lowest measured temperatures. These indicate that below T_M there could be the onset of a FM component, as also found in some other Tb-based compounds [47]. There is a lack of hysteresis at T_N between zero-field-cooled (ZFC) and FC measurements, but there is a small splitting of the two curves in the vicinity of T_M for $H \parallel c$. The overall shape of the $\chi(T)$ curves is similar for both $H \parallel c$ and $H \parallel ab$, but the larger values for $H \parallel c$ indicate that the c axis is the easy axis.

For fields applied along both directions, $\chi(T)$ follows Curie-Weiss behavior from 300 K down to around 60 K, as shown in the inset of Fig. 2(b). These were fitted to a modified Curie-Weiss law: $\chi = \chi_0 + C/(T - \theta_P)$ from 100 to 300 K, where χ_0 is the temperature-independent susceptibility, C is the Curie constant, and θ_P is the Curie-Weiss temperature. For

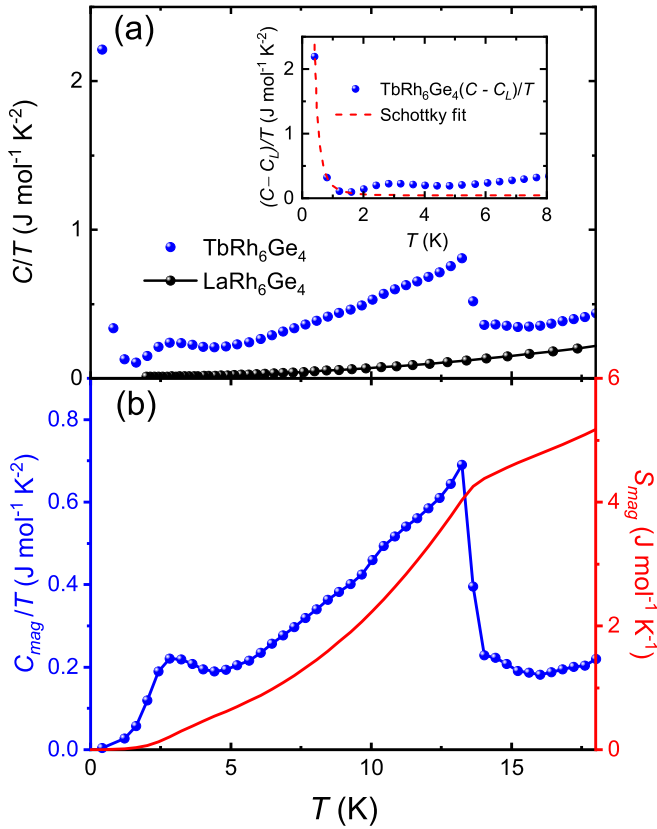


FIG. 3. (a) Temperature dependence of the specific heat as C/T of TbRh_6Ge_4 (blue) and LaRh_6Ge_4 (black). The inset shows the low-temperature behavior, where the red dashed line shows the results from fitting to a nuclear Schottky contribution at low temperatures. (b) Temperature dependence of the magnetic contribution to the specific heat C_{mag}/T and magnetic entropy S_{mag} , where C_{mag}/T is obtained from subtracting both the estimated lattice and nuclear Schottky parts.

$H \parallel c$, an effective magnetic moment of $\mu_{\text{eff}} = 9.73 \mu_{\text{B}}/\text{Tb}$ and a Curie-Weiss temperature $\theta_p^c = 21.50 \text{ K}$ were obtained, while for $H \parallel ab$, $\mu_{\text{eff}} = 9.89 \mu_{\text{B}}/\text{Tb}$ and $\theta_p^{ab} = -53.0 \text{ K}$. The effective magnetic moments for both orientations are close to the expected value of $9.70 \mu_{\text{B}}$ for a Tb^{3+} ion with $J = 6$. The anisotropy of θ_p suggests that there are in-plane antiferromagnetic couplings, with ferromagnetic coupling along the c axis (Tb chains).

Figure 3(a) displays the temperature dependence of the specific heat as C/T of TbRh_6Ge_4 and LaRh_6Ge_4 down to 0.4 K in zero field. A clear bulk phase transition is observed in TbRh_6Ge_4 at $T_N = 12.7 \text{ K}$, in line with that of $\rho(T)$ and $\chi(T)$. In addition, another smaller anomaly is observed at $T_M = 2.8 \text{ K}$, and below 1.6 K there is a sharp upturn likely corresponding to a nuclear Schottky contribution. In order to estimate the magnetic contribution (C_{mag}), it is necessary to subtract both the lattice contribution (C_L), which was estimated from the specific heat of LaRh_6Ge_4 , and the nuclear Schottky contribution $C_N = A_N/T^2$, obtained from fitting the data below 1.6 K with $A_N = 0.15 \text{ J K mol}^{-1}$ [inset of Fig. 3(a)]. The temperature dependences of the magnetic specific heat C_{mag}/T and magnetic entropy per Tb S_{mag} are displayed in Fig. 3(b). S_{mag} at T_N is around $0.75R\ln 2$, while

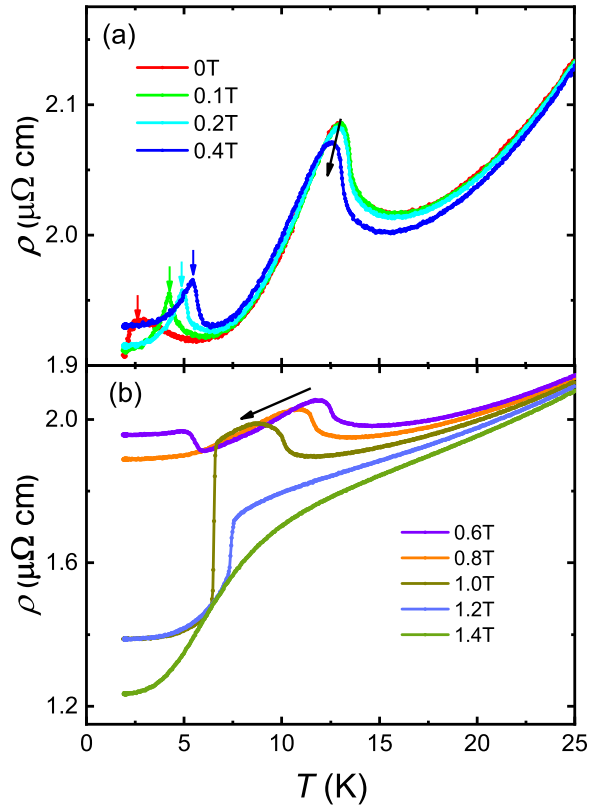


FIG. 4. Temperature dependence of the resistivity of TbRh_6Ge_4 in different applied magnetic fields (a) below 0.4 T and (b) above 0.6 T, applied parallel to the easy c axis, with the current also along the same direction.

it reaches $R\ln 2$ at around 20 K. Such a reduced entropy at T_N could be due to the presence of frustration-induced fluctuations.

B. In-field measurements

Figure 4 displays the low-temperature resistivity of TbRh_6Ge_4 in different magnetic fields applied along the c axis. With increasing magnetic field, the transition at T_N is continuously suppressed to lower temperatures, and the lower transition gradually increases, in line with the former being an AFM transition and the latter having a ferromagnetic component. In 0.8 T, only the transition at T_N is observed, and upon increasing the field to 1 T, a new low-temperature transition appears at which there is an abrupt drop of $\rho(T)$. This field-induced transition shifts to higher temperatures with increasing field, and disappears above 1.4 T.

The field dependence of the magnetization of TbRh_6Ge_4 at 2 K is displayed in Fig. 5, for fields applied along the c axis and in the ab plane. There is strong magnetic anisotropy, where the magnetization for $H \parallel c$ is much larger than that for $H \perp c$. For $H \perp c$, there is a gradual increase of the magnetization, reaching about $0.6 \mu_{\text{B}}/\text{Tb}$ at 1.5 T, where there is a weak anomaly around which there is slight hysteresis between up-sweep and down-sweep measurements. For $H \parallel c$, as shown in the inset there is a hysteresis loop about zero field, with a finite remanent magnetization, again showing that the low-temperature phase below T_M has a finite net

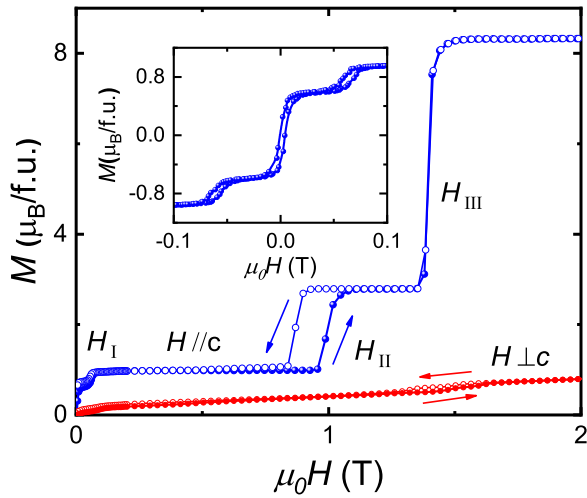


FIG. 5. Field dependence of the magnetization of TbRh_6Ge_4 at 2 K for $H \parallel c$ and $H \perp c$, measured upon sweeping the field up and down. The inset shows the magnetization at low fields for $H \parallel c$.

magnetization with domains that reorientate in small applied c -axis fields. Upon further increasing the field, there are three successive metamagnetic transitions with abrupt jumps in the magnetization, separated by plateaus which only exhibit a weak change of magnetization with field. Upon sweeping the field up, the first transition is at $\mu_0 H_I = 0.06$ T with weak hysteresis between up- and downfield sweeps, and the magnetization reaches $0.98 \mu_B/\text{Tb}$ at 0.1 T. The second transition is at $\mu_0 H_{II} = 0.95$ T, where there is more extended hysteresis and the magnetization is $2.78 \mu_B/\text{Tb}$ at 1 T. At $\mu_0 H_{III} = 1.5$ T, there is another abrupt metamagnetic transition, above which the magnetization reaches $8.3 \mu_B/\text{Tb}$, corresponding to the saturation magnetization M_s . The magnetization in the plateaus above H_I and H_{II} correspond to $M_s/9$ and $M_s/3$, respectively. These suggest that the metamagnetic transitions correspond to spin-flip transitions, with the spins remaining orientated along the c axis. Meanwhile, above H_{III} , the system is in the spin-polarized state.

The isothermal magnetization as a function of field along the c axis at several temperatures is displayed in Fig. 6(a), which was cooled in zero field and then measured upon sweeping the field both up and down. At 6 K, the first metamagnetic transition is not observed and instead there is a smooth increase of magnetization in this region, while above 8 K, there is only a single metamagnetic transition. Above T_N at 15 K, there is a smooth increase of magnetization with field, as expected in the paramagnetic state.

Figure 6(b) shows the magnetic susceptibility of TbRh_6Ge_4 for different magnetic fields with $H \parallel c$. With increasing field, T_N is suppressed to lower temperatures, with the corresponding peak becoming broader (indicated by the black dashed arrow). The low-temperature increase of $\chi(T)$ is also suppressed upon increasing the field up to 0.5 T. Upon further increasing the field above 1 T ($H > H_{II}$), a new transition appears in the magnetically ordered state, below which there is a sharp increase in $\chi(T)$, which also shifts to higher temperature with increasing field (magenta arrows). In a 1.3 T field, only a single transition is observed (green

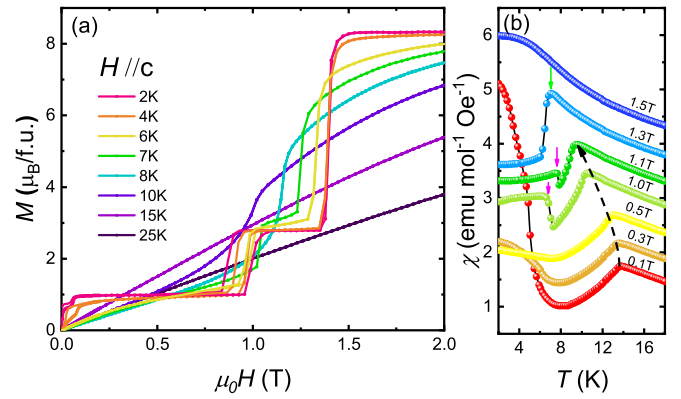


FIG. 6. (a) Field dependence of the magnetization of TbRh_6Ge_4 at various temperatures for $H \parallel c$. (b) Temperature dependence of $\chi(T)$ measured in fields applied parallel to the c axis. $\chi(T)$ in consecutive fields are shifted vertically by 0.5 emu/mol Oe for clarity. The black dashed arrow denotes the trend of T_N , while the magenta and green downward arrows mark the two transitions to the field-induced phases.

arrow), which is in good agreement with the $\rho(T)$ data in applied fields.

The specific heat (as C/T) in various fields for $H \parallel c$ are shown in Fig. 7(a), where T_N is suppressed rapidly to lower temperatures with increasing magnetic field. The weaker anomaly at T_M shifts to higher temperatures and becomes less pronounced, which is consistent with $\chi(T)$ in Fig. 6(b). At higher fields (>0.6 T) another anomaly is observed (magenta arrows), which persists up to at least 1 T, being consistent with the field-induced transition in $\chi(T)$. Figure 7(b) shows the field dependence of $C(H)/T$ at various temperatures. There

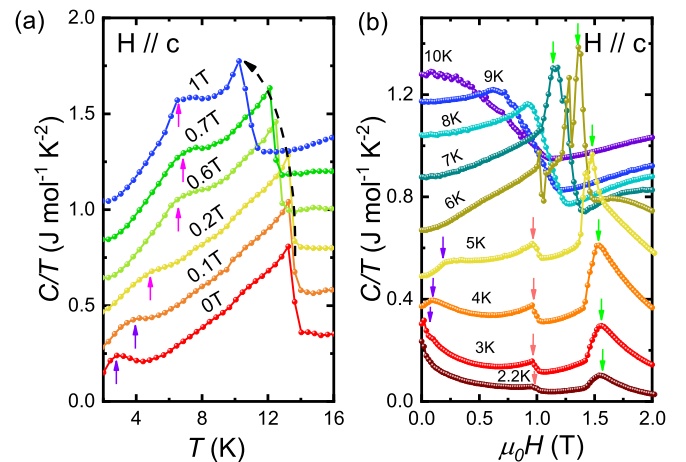


FIG. 7. (a) Temperature dependence of the specific heat of TbRh_6Ge_4 in both zero field and different fields applied along the c axis. Data at consecutive fields are shifted vertically by $0.2 \text{ J mol}^{-1} \text{ K}^{-2}$ for clarity. The black dashed arrow denotes the trend of T_N , while the purple and magenta arrows correspond to T_M and the field-induced transition, respectively. (b) Field dependence of C/T measured at various temperatures for $H \parallel c$. Data at consecutive temperatures are shifted vertically by $0.05 \text{ J mol}^{-1} \text{ K}^{-2}$ for clarity. The vertical arrows mark the various metamagnetic transitions described in the text.

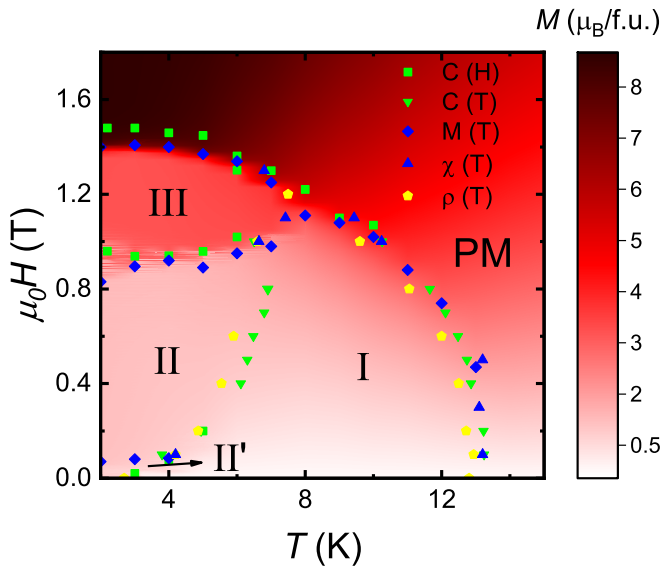


FIG. 8. Magnetic field-temperature phase diagram of TbRh_6Ge_4 for $H \parallel c$. The color plot represents the magnitude of the magnetization, while the symbols correspond to transitions determined from different quantities labeled in the legend.

are multiple anomalies, which are consistent with the metamagnetic transitions observed in the magnetization.

IV. DISCUSSION

TbRh_6Ge_4 crystallizes in a hexagonal structure with triangular lattices of Tb ions stacked along the c axis. The relatively short Tb-Tb separation along the c axis of 3.81 Å, compared to 7.15 Å within the ab plane, together with the strong easy axis magnetic anisotropy, suggests that TbRh_6Ge_4 can be considered as consisting of coupled Ising chains of Tb atoms. The anisotropic Curie-Weiss temperatures of $\theta_P = 21.5$ K ($H \parallel c$) and -53.0 K ($H \parallel ab$) also indicate that there may be predominantly ferromagnetic intrachain interactions (along the c axis), and antiferromagnetic interchain interactions within the ab plane. The magnetic entropy at T_N of $0.75R\ln 2$ together with a sizable saturation magnetization at low temperatures points to the magnetic properties being governed by a ground state doublet arising from the splitting of 13-fold degenerate $J = 6$ Hund's rule multiplet by the hexagonal CEF. Here the CEF splits the multiplet into four doublets and five nonmagnetic singlets, and the large value of the saturation magnetization along the c axis $M_s \approx 8.3 \mu_B/\text{Tb}$ indicates that the ground state CEF wave function likely predominantly consists of the $|m_J = \pm 5\rangle$ states, with only a small admixture of $|m_J = \mp 1\rangle$. However, determination of the CEF level scheme and ground state wave functions requires additional probes of the CEF excitations, such as inelastic neutron scattering.

TbRh_6Ge_4 exhibits complex magnetism, where in zero field there are two magnetic transitions at $T_N = 12.7$ K and $T_M = 2.8$ K, and there are multiple metamagnetic transitions in applied c axis magnetic fields. Based on all our results, we constructed the H - T phase diagram of TbRh_6Ge_4 ($H \parallel c$), which is displayed in Fig. 8, and the phase boundaries

derived from different measurements coincide well. The region labeled *I* corresponds to the AFM phase below T_N , while *II'* denotes the magnetic phase below T_M , which has both ferromagnetic and AFM components. In the two field-induced magnetic phases *II* and *III*, there are plateaus where the magnetization changes little with field, and the values correspond to integer fractions of the saturation magnetization M_s of $M_s/9$ and $M_s/3$, respectively. This suggests that these metamagnetic transitions correspond to spin-flip transitions of Ising spins that remain strongly constrained to lie along the c axis by the magnetocrystalline anisotropy. Note that the net magnetization in the *II'* phase is slightly less than the $M_s/9$ of phase *II*, and only a very small field is necessary to switch between these. This suggests that the magnetic structures may be very similar between these phases. Meanwhile, upon further increasing the field above H_{III} , the system is spin polarized where all the spins are aligned.

We note that magnetization plateaus at $M_s/9$ and $M_s/3$ are also observed in DyAlGa [35] and HoAlGa [36], which have triangular lattices of rare-earth ions with strong Ising anisotropy. Neutron diffraction measurements reveal that in all the phases the spins are orientated along the c axis, and the spins within each Dy/Ho triangle are frustrated, with two aligned spins and one antialigned spin. In the zero-field antiferromagnetic phase, the spins in each chain are antiferromagnetically aligned along the c axis, leading to a magnetic structure with zero net moment, while in the phase with $M_s/3$, one-third of the chains have ferromagnetically aligned spins. Meanwhile, the magnetic cell of the phase with $M_s/9$ has a larger periodicity, repeating every six layers. On the other hand, while in both DyAlGa and HoAlGa the zero-field structures all have no net moment, in TbRh_6Ge_4 there is a ferromagnetic component in the zero-field phase below T_M . Furthermore, the Curie-Weiss analysis suggests predominantly ferromagnetic interactions along the c axis, as compared to the antiferromagnetic chains of DyAlGa and HoAlGa . Therefore, microscopic probes of the magnetic structure of TbRh_6Ge_4 such as neutron diffraction are necessary to check whether the magnetic structures are analogous to the aforementioned compounds, or whether similar magnetization plateaus can be realized with *ferromagnetic* Ising chains. Note that in $\text{Ca}_3\text{Co}_2\text{O}_6$ there are predominantly ferromagnetic intrachain interactions, but an antiferromagnetic magnetic structure modulated along the c axis is realized by different antiferromagnetic interchain exchange interactions [48,49].

V. CONCLUSION

In summary, we have synthesized single crystals of TbRh_6Ge_4 , where the Tb atoms form a triangular lattice in the ab plane and a chain structure along the c axis. Unlike the ferromagnetic quantum critical system CeRh_6Ge_4 , TbRh_6Ge_4 orders antiferromagnetically in zero field below $T_N = 12.7$ K, and exhibits a second transition below $T_M = 2.8$ K, and this magnetic phase also incorporates a ferromagnetic component. Magnetization measurements show that the c axis is the easy axis in both the paramagnetic and magnetically ordered phases, and the field-dependent measurements reveal phases with magnetization plateaus at $1/9$ and $1/3$ of the saturated

magnetization. Our findings indicate complex magnetism in TbRh_6Ge_4 , where antiferromagnetic interactions between tri-angulantly arranged Tb chains suggest that there is strong magnetic frustration. In order to characterize the microscopic nature of the magnetism in TbRh_6Ge_4 , it is of particular interest to probe the magnetic structure and excitations with microscopic probes such as neutron and x-ray scattering.

ACKNOWLEDGMENTS

This work was supported by the National Key R&D Program of China (Grant No. 2022YFA1402200), the National Natural Science Foundation of China (Grants No. 12034017, No. 12174332, No. 11974306, and No. 12222410), and the Key R&D Program of Zhejiang Province, China (Grant No. 2021C01002).

-
- [1] L. Balents, Spin liquids in frustrated magnets, *Nature (London)* **464**, 199 (2010).
- [2] T.-H. Han, J. S. Helton, S. Chu, D. G. Nocera, J. A. Rodriguez-Rivera, C. Broholm, and Y. S. Lee, Fractionalized excitations in the spin-liquid state of a kagome-lattice antiferromagnet, *Nature (London)* **492**, 406 (2012).
- [3] O. A. Starykh, Unusual ordered phases of highly frustrated magnets: A review, *Rep. Prog. Phys.* **78**, 052502 (2015).
- [4] A. V. Chubukov and D. I. Golosov, Quantum theory of an antiferromagnet on a triangular lattice in a magnetic field, *J. Phys.: Condens. Matter* **3**, 69 (1991).
- [5] D. C. Cabra, A. Honecker, and P. Pujol, Magnetization Curves of Antiferromagnetic Heisenberg Spin $\frac{1}{2}$ Ladders, *Phys. Rev. Lett.* **79**, 5126 (1997).
- [6] M. Oshikawa, M. Yamanaka, and I. Affleck, Magnetization Plateaus in Spin Chains: “Haldane Gap” for Half-Integer Spins, *Phys. Rev. Lett.* **78**, 1984 (1997).
- [7] K. Totsuka, Magnetization plateau in the $S = \frac{1}{2}$ Heisenberg spin chain with next-nearest-neighbor and alternating nearest-neighbor interactions, *Phys. Rev. B* **57**, 3454 (1998).
- [8] R. Chen, J. F. Wang, Z. W. Ouyang, Z. Z. He, S. M. Wang, L. Lin, J. M. Liu, C. L. Lu, Y. Liu, C. Dong, C. B. Liu, Z. C. Xia, A. Matsuo, Y. Kohama, and K. Kindo, Magnetic field induced ferroelectricity and half magnetization plateau in polycrystalline $R_2V_2O_7$ ($R = \text{Ni, Co}$), *Phys. Rev. B* **98**, 184404 (2018).
- [9] L. A. Fenner, A. A. Dee, and A. S. Wills, Non-collinearity and spin frustration in the itinerant kagome ferromagnet Fe_3Sn_2 , *J. Phys.: Condens. Matter* **21**, 452202 (2009).
- [10] C. Sürgers, G. Fischer, P. Winkel, and H. v. Löhneysen, Large topological Hall effect in the non-collinear phase of an antiferromagnet, *Nat. Commun.* **5**, 3400 (2014).
- [11] T. Kurumaji, T. Nakajima, M. Hirschberger, A. Kikkawa, Y. Yamasaki, H. Sagayama, H. Nakao, Y. Taguchi, T.-H. Arima, and Y. Tokura, Skyrmion lattice with a giant topological Hall effect in a frustrated triangular-lattice magnet, *Science* **365**, 914 (2019).
- [12] Y. Yamashita and K. Ueda, Spin-Driven Jahn-Teller Distortion in a Pyrochlore System, *Phys. Rev. Lett.* **85**, 4960 (2000).
- [13] M. Onoda and J. Hasegawa, A distortion of pseudotetramers coupled with the Jahn-Teller effect in the geometrically frustrated spinel system CdV_2O_4 , *J. Phys.: Condens. Matter* **15**, L95 (2003).
- [14] M. C. Kemei, P. T. Barton, S. L. Moffitt, M. W. Gaultois, J. A. Kurzman, R. Seshadri, M. R. Suchomel, and Y.-I. Kim, Crystal structures of spin-Jahn-Teller-ordered MgCr_2O_4 and ZnCr_2O_4 , *J. Phys.: Condens. Matter* **25**, 326001 (2013).
- [15] T. Inami, Y. Ajiro, and T. Goto, Magnetization process of the triangular lattice antiferromagnets, $\text{RbFe}(\text{MoO}_4)_2$ and $\text{CsFe}(\text{SO}_4)_2$, *J. Phys. Soc. Jpn.* **65**, 2374 (1996).
- [16] T. Ono, H. Tanaka, H. Aruga Katori, F. Ishikawa, H. Mitamura, and T. Goto, Magnetization plateau in the frustrated quantum spin system Cs_2CuBr_4 , *Phys. Rev. B* **67**, 104431 (2003).
- [17] H. Nakano and T. Sakai, Magnetization process of the spin-1/2 triangular-lattice Heisenberg antiferromagnet with next-nearest-neighbor interactions — Plateau or nonplateau —, *J. Phys. Soc. Jpn.* **86**, 114705 (2017).
- [18] H. Kageyama, K. Yoshimura, R. Stern, N. V. Mushnikov, K. Onizuka, M. Kato, K. Kosuge, C. P. Slichter, T. Goto, and Y. Ueda, Exact Dimer Ground State and Quantized Magnetization Plateaus in the Two-Dimensional Spin System $\text{SrCu}_2(\text{BO}_3)_2$, *Phys. Rev. Lett.* **82**, 3168 (1999).
- [19] S. Yoshii, T. Yamamoto, M. Hagiwara, S. Michimura, A. Shigekawa, F. Iga, T. Takabatake, and K. Kindo, Multi-step Magnetization Plateaus in the Shastry-Sutherland System TbB_4 , *Phys. Rev. Lett.* **101**, 087202 (2008).
- [20] M. E. Zhitomirsky, A. Honecker, and O. A. Petrenko, Field Induced Ordering in Highly Frustrated Antiferromagnets, *Phys. Rev. Lett.* **85**, 3269 (2000).
- [21] Y. Tsujimoto, Y. Baba, N. Oba, H. Kageyama, T. Fukui, Y. Narumi, K. Kindo, T. Saito, M. Takano, Y. Ajiro, and K. Yoshimura, 1/3 magnetization plateau in spin-1/2 square lattice antiferromagnet $(\text{CuBr})\text{Sr}_2\text{Nb}_3\text{O}_{10}$, *J. Phys. Soc. Jpn.* **76**, 063711 (2007).
- [22] S. Nishimoto, N. Shibata, and C. Hotta, Controlling frustrated liquids and solids with an applied field in a kagome Heisenberg antiferromagnet, *Nat. Commun.* **4**, 2287 (2013).
- [23] H. Nakano, Y. Hasegawa, and T. Sakai, Magnetization jump in the magnetization process of the spin-1/2 Heisenberg antiferromagnet on a distorted square-kagome lattice, *J. Phys. Soc. Jpn.* **84**, 114703 (2015).
- [24] S. Capponi, O. Derzhko, A. Honecker, A. M. Läuchli, and J. Richter, Numerical study of magnetization plateaus in the spin- $\frac{1}{2}$ kagome Heisenberg antiferromagnet, *Phys. Rev. B* **88**, 144416 (2013).
- [25] J. Wang, M. Tokunaga, Z. Z. He, J. I. Yamaura, A. Matsuo, and K. Kindo, High magnetic field induced phases and half-magnetization plateau in the $S = 1$ kagome compound $\text{Ni}_3\text{V}_2\text{O}_8$, *Phys. Rev. B* **84**, 220407(R) (2011).
- [26] R. Shirakami, H. Ueda, H. O. Jeschke, H. Nakano, S. Kobayashi, A. Matsuo, T. Sakai, N. Katayama, H. Sawa, K. Kindo, C. Michioka, and K. Yoshimura, Two magnetization plateaus in the kagome fluoride $\text{Cs}_2\text{LiTi}_3\text{F}_{12}$, *Phys. Rev. B* **100**, 174401 (2019).
- [27] T. T. A. Lummen, C. Strohm, H. Rakoto, and P. H. M. van Loosdrecht, Mapping the magnetic phase diagram of the frustrated metamagnet CuFeO_2 , *Phys. Rev. B* **81**, 224420 (2010).

- [28] F. Wang and A. Vishwanath, Spin Phonon Induced Collinear Order and Magnetization Plateaus in Triangular and Kagome Antiferromagnets: Applications to CuFeO_2 , *Phys. Rev. Lett.* **100**, 077201 (2008).
- [29] W. Shiramura, K. Takatsu, H. Tanaka, K. Kamishima, M. Takahashi, H. Mitamura, and T. Goto, High-field magnetization processes of double spin chain systems KCuCl_3 and TiCuCl_3 , *J. Phys. Soc. Jpn.* **66**, 1900 (1997).
- [30] K. Hida and I. Affleck, Quantum vs classical magnetization plateaus of $S=1/2$ frustrated Heisenberg chains, *J. Phys. Soc. Jpn.* **74**, 1849 (2005).
- [31] A. Metavitsiadis, C. Psaroudaki, and W. Brenig, Enhancement of magnetization plateaus in low-dimensional spin systems, *Phys. Rev. B* **101**, 235143 (2020).
- [32] X. Y. Yao, S. Dong, and J.-M. Liu, Steplike magnetization of spin chains in a triangular lattice: Monte Carlo simulations, *Phys. Rev. B* **73**, 212415 (2006).
- [33] W. Shiramura, K.-I. Takatsu, B. Kurniawan, H. Tanaka, H. Uekusa, Y. Ohashi, K. Takizawa, H. Mitamura, and T. Goto, Magnetization plateaus in NH_4CuCl_3 , *J. Phys. Soc. Jpn.* **67**, 1548 (1998).
- [34] Z. He and W. Cheng, Magnetic phase diagram of an Ising spin-chain system $\alpha\text{-CoV}_2\text{O}_6$ with $1/3$ magnetization plateau, *J. Magn. Magn. Mater.* **362**, 27 (2014).
- [35] D. Gignoux, D. Schmitt, J. Voiron, F. Zhang, E. Bauer, and G. Schaudy, Magnetic phase diagram of the hexagonal DyAlGa compound, *J. Alloys Compd.* **191**, 139 (1993).
- [36] A. Ball, D. Gignoux, D. Schmitt, F. Zhang, and M. Reehuis, Field induced magnetic structures in hexagonal HoAlGa , *J. Magn. Magn. Mater.* **110**, 343 (1992).
- [37] A. Ball, D. Gignoux, A. Murani, and D. Schmitt, Crystal field and complex phase diagram in hexagonal PrGa_2 , *Phys. B: Condens. Matter* **190**, 214 (1993).
- [38] A. Garnier, D. Gignoux, D. Schmitt, and T. Shigeoka, Evidence of mixed magnetic phases in TbRu_2Ge_2 , *Phys. Rev. B* **57**, 5235 (1998).
- [39] D. Voßwinkel, O. Niehaus, U. C. Rodewald, and R. Pöttgen, Bismuth flux growth of CeRh_6Ge_4 and CeRh_2Ge_2 single crystals, *Z. Naturforsch. B* **67**, 1241 (2012).
- [40] D. Voßwinkel, O. Niehaus, and R. Pöttgen, New rhodium-rich germanides RERh_6Ge_4 ($\text{RE} = \text{Y, La, Pr, Nd, Sm-Lu}$), *Z. Anorg. Allg. Chem.* **639**, 2623 (2013).
- [41] E. Matsuoka, C. Hondo, T. Fujii, A. Oshima, H. Sugawara, T. Sakurai, H. Ohta, F. Kneidinger, L. Salamakha, H. Michor, and E. Bauer, Ferromagnetic transition at 2.5 K in the hexagonal Kondo-lattice compound CeRh_6Ge_4 , *J. Phys. Soc. Jpn.* **84**, 073704 (2015).
- [42] B. Shen, Y. Zhang, Y. Komijani, M. Nicklas, R. Borth, A. Wang, Y. Chen, Z. Nie, R. Li, X. Lu, H. Lee, M. Smidman, F. Steglich, P. Coleman, and H. Q. Yuan, Strange-metal behaviour in a pure ferromagnetic Kondo lattice, *Nature (London)* **579**, 51 (2020).
- [43] A. Wang, F. Du, Y. J. Zhang, D. Graf, B. Shen, Y. Chen, Y. Liu, M. Smidman, C. Cao, F. Steglich, and H. Q. Yuan, Localized $4f$ -electrons in the quantum critical heavy fermion ferromagnet CeRh_6Ge_4 , *Sci. Bull.* **66**, 1389 (2021).
- [44] Y. Wu, Y. Zhang, F. Du, B. Shen, H. Zheng, Y. Fang, M. Smidman, C. Cao, F. Steglich, H. Q. Yuan, J. D. Denlinger, and Y. Liu, Anisotropic c - f Hybridization in the Ferromagnetic Quantum Critical Metal CeRh_6Ge_4 , *Phys. Rev. Lett.* **126**, 216406 (2021).
- [45] J. W. Shu, D. T. Adroja, A. D. Hillier, Y. J. Zhang, Y. X. Chen, B. Shen, F. Orlandi, H. C. Walker, Y. Liu, C. Cao, F. Steglich, H. Q. Yuan, and M. Smidman, Magnetic order and crystalline electric field excitations of the quantum critical heavy-fermion ferromagnet CeRh_6Ge_4 , *Phys. Rev. B* **104**, L140411 (2021).
- [46] H. H. Uhlig, *The Theory of the Properties of Metals and Alloys*. (American Chemical Society, Washington, DC, 1959), Vol. 81, pp. 3808–3808.
- [47] A. D. Chinchure, M. Doerr, G. Behr, S. Dhar, R. Nagarajan, V. Marathe, M. Loewenhaupt, and L. Gupta, Magnetic properties of $\text{R}_2\text{Re}_2\text{Si}_2\text{C}$ ($\text{R}=\text{Tb}$ and Dy), *Phys. B: Condens. Matter* **299**, 135 (2001).
- [48] S. Aasland, H. Fjellvåg, and B. Hauback, Magnetic properties of the one-dimensional $\text{Ca}_3\text{Co}_2\text{O}_6$, *Solid State Commun.* **101**, 187 (1997).
- [49] S. Agrestini, L. C. Chapon, A. Daoud-Aladine, J. Schefer, A. Gukasov, C. Mazzoli, M. R. Lees, and O. A. Petrenko, Nature of the Magnetic Order in $\text{Ca}_3\text{Co}_2\text{O}_6$, *Phys. Rev. Lett.* **101**, 097207 (2008).